J|A|C|S ARTICLES

Published on Web 04/30/2010

Optimizing Single-Molecule Conductivity of Conjugated Organic Oligomers with Carbodithioate Linkers

Yangjun Xing,[†] Tae-Hong Park,[‡] Ravindra Venkatramani,[§] Shahar Keinan,[§] David N. Beratan,*[,§,#] Michael J. Therien,*[,§] and Eric Borguet*[,†]

Department of Chemistry, Temple University, Philadelphia, Pennsylvania 19122, Department of Chemistry, University of Pennsylvania, Philadelphia, Pennsylvania 19104, Departments of Chemistry, Biochemistry, and Physics, Duke University, Durham, North Carolina 27708, and Department of Chemistry, French Family Science Center, Duke University, Durham, North Carolina 27708

Received November 16, 2009; E-mail: eborguet@temple.edu; michael.therien@duke.edu; david.beratan@duke.edu

Abstract: In molecular electronics, the linker group, which attaches the functional molecular core to the electrode, plays a crucial role in determining the overall conductivity of the molecular junction. While much focus has been placed on optimizing molecular core conductivity, there have been relatively few attempts at designing optimal linker groups to metallic or semiconducting electrodes. The vast majority of molecular electronic studies use thiol linker groups; work probing alternative amine linker systems has only recently been explored. Here, we probe single-molecule conductances in phenylene−ethynylene molecules terminated with thiol and carbodithioate linkers, experimentally using STM break-junction methods and theoretically using a nonequilibrium Green's function approach. Experimental studies demonstrate that the carbodithioate linker augments electronic coupling to the metal electrode and lowers the effective barrier for charge transport relative to the conventional thiol linker, thus enhancing the conductance of the linker−phenylene−ethynylene−linker unit; these data underscore that phenylene−ethynylene-based structures are more highly conductive than originally appreciated in molecular electronics applications. The theoretical analysis shows that the nature of sulfur hybridization in these species is responsible for the order-of-magnitude increased conductance in carbodithioate-terminated systems relative to identical conjugated structures that feature classic thiol linkers, independent of the mechanism of charge transport. Interestingly, in these systems, the tunneling current is not dominated by the frontier molecular orbitals. While barriers $< k_B T$ are expected to produce low β values, we show that the competition between tunneling and resonant transport processes allows barriers $\gg k_B T$ to produce the low β values seen in our experiments. Taken together, these experimental and theoretical studies indicate a promising role for carbodithioate-based connectivity in molecular-scale electronics applications involving metallic and semiconducting electrodes.

Introduction

The development of molecular connects to metallic and semiconducting electrodes that possess controllable properties is a major milestone in the molecular electronics roadmap.[1−4] Recent years have seen great theoretical[5−10] and experimental[11−18] progress in the field of molecular electronics and most recently a real molecule-based memory device has even been fabricated.[19]

[†] Temple University.
[‡] University of Pennsylvania.
[§] Department of Chemistry, Duke University.
[#] Department of Biochemistry and Physics, Duke University.

(1) Aviram, A.; Ratner, M. A. *Chem. Phys. Lett.* **1974**, *29*, 277–283.
(2) Frank, D. J.; Dennard, R. H.; Nowak, E.; Solomon, P. M.; Taur, Y.; Wong, H. S. P. *Proc. IEEE* **2001**, *89*, 259–288.
(3) Heath, J. R.; Ratner, M. A. *Phys. Today* **2003**, *56*, 43–49.
(4) Lu, W.; Lieber, C. M. *Nat. Mater.* **2007**, *6*, 841–850.
(5) Cohen, R.; Stokbro, K.; Martin, J. M. L.; Ratner, M. A. *J. Phys. Chem. C* **2007**, *111*, 14893–14902.
(6) Fan, F. R. F.; Lai, R. Y.; Cornil, J.; Karzazi, Y.; Bredas, J. L.; Cai, L. T.; Cheng, L.; Yao, Y. X.; Price, D. W.; Dirk, S. M.; Tour, J. M.; Bard, A. J. *J. Am. Chem. Soc.* **2004**, *126*, 2568–2573.
(7) Heimel, G.; Romaner, L.; Bredas, J. L.; Zojer, E. *Phys. Rev. Lett.* **2006**, *96*, 196806.
(8) Piccinin, S.; Selloni, A.; Scandolo, S.; Car, R.; Scoles, G. *J. Chem. Phys.* **2003**, *119*, 6729–6735.
(9) Xue, Y.; Ratner, M. A. *Phys. Rev. B* **2003**, *68*, 115406.
(10) Tomfohr, J.; Sankey, O. F. *J. Chem. Phys.* **2004**, *120*, 1542–1554.
(11) Cui, X. D.; Primak, A.; Zarate, X.; Tomfohr, J.; Sankey, O. F.; Moore, A. L.; Moore, T. A.; Gust, D.; Harris, G.; Lindsay, S. M. *Science* **2001**, *294*, 571–574.
(12) Dadosh, T.; Gordin, Y.; Krahne, R.; Khivrich, I.; Mahalu, D.; Frydman, V.; Sperling, J.; Yacoby, A.; Bar-Joseph, I. *Nature* **2005**, *436*, 677–680.
(13) Davis, W. B.; Svec, W. A.; Ratner, M. A.; Wasielewski, M. R. *Nature* **1998**, *396*, 60–63.
(14) Donhauser, Z. J.; Mantooth, B. A.; Kelly, K. F.; Bumm, L. A.; Monnell, J. D.; Stapleton, J. J.; Price, D. W.; Rawlett, A. M.; Allara, D. L.; Tour, J. M.; Weiss, P. S. *Science* **2001**, *292*, 2303–2307.
(15) Li, C.; Pobelov, I.; Wandlowski, T.; Bagrets, A.; Arnold, A.; Evers, F. *J. Am. Chem. Soc.* **2008**, *130*, 318–326.
(16) Reed, M. A.; Zhou, C.; Muller, C. J.; Burgin, T. P.; Tour, J. M. *Science* **1997**, *278*, 252–254.
(17) Reichert, J.; Ochs, R.; Beckmann, D.; Weber, H. B.; Mayor, M.; von Lohneysen, H. *Phys. Rev. Lett.* **2002**, *88*, 176804.
(18) Xu, B. Q.; Tao, N. J. J. *Science* **2003**, *301*, 1221–1223.
(19) Green, J. E.; Choi, J. W.; Boukai, A.; Bunimovich, Y.; Johnston-Halperin, E.; DeIonno, E.; Luo, Y.; Sheriff, B. A.; Xu, K.; Shin, Y. S.; Tseng, H. R.; Stoddart, J. F.; Heath, J. R. *Nature* **2007**, *445*, 414–417.

 10.1021/ja909559m

A key challenge in developing functional molecular connects is to build a nanoscale electrode−molecule−electrode system that can be probed experimentally in a repeated and controlled fashion. At least one of the electrodes should be of nanoscale dimensions to ensure that one molecule (or at most a few molecules) is trapped between electrodes and probed. Researchers have created a number of methods to make nanoelectrodes, including electro-migrated junctions,[20,21] mechanical break-junctions,[17] mixed self-assembled monolayers (SAMs),[11] and scanning tunneling microscopy (STM) break-junctions.[18,22] Since nanoscale molecular conductance is affected by many factors, including the conformation of the molecules, the angle of linker-electrode bonds, and the environment,[23−26] individual measurements may therefore fluctuate by orders of magnitude,[14,24,27] underscoring the importance of repetitive measurements to provide statistically significant results. The STM break-junction method,[18] one of the most widely used techniques for measuring single-molecule conductivity, is designed to create, repeatedly and rapidly, nanoscale electrode−molecule−electrode systems so that thousands of experiments can be conducted in a few hours or less.[18,22,28−34] A closely related challenge presented by single-molecule conductance data is to determine the relative influence of the molecular "core" and the molecular "interconnects" on observed currents; such analyses are necessary to elucidate important structure−function relationships necessary to design molecular electronic elements having the desired functionality.

Charge transport through metal−molecule−metal (m−M−m) junctions has been investigated by measuring conductance (or resistance) as a function of distance.[10,26,29,31,35−41] In the tunneling regime where molecular junctions usually operate,[26,35,40] the junction resistance (R) increases approximately exponentially with molecular length L: $R = R_0\exp(\beta \mathrm{L})$. Here R_0 is an effective contact resistance and β is a constant, which depends on the structure of the molecular backbone. An approximately exponential decay of conductance with bridge length best describes the bridge mediated tunneling (superexchange) in donor-bridge-acceptor (D−B−A) systems where the donor/acceptor energies are off resonance with the bridge. While single-step tunneling is mediated by eigenstates of the bridging molecule, these states are populated only virtually, and the tunneling rate decays exponentially with the bridge length. On the other hand, when donor/acceptor energy levels are resonant with those of the bridge, electrons (or holes) are injected into the states of the bridging molecule, and charge transfer (CT) from D to A takes place via populated bridge states. In this case, the donor−acceptor distance dependence of the charge transfer rate constant is very soft. Thus, small values of β are consistent with transport via carrier injection. It should be emphasized that the parameter β described above, and used throughout this paper, is a decay constant for transmission across a barrier extracted from fitting an exponential to experimental (or computed) resistance values. It is not the same as the superexchange decay constant, which we denote β_{SE}. The latter is defined only in the pure superexchange limit and holds no meaning when carriers populate the bridge states. Thus $\beta = \beta_{\mathrm{SE}}$ only in the pure superexchange limit.

π-Symmetry backbones present lower tunneling barriers than σ-bonded systems, thus π-conjugated molecules have been found to have much smaller β values than saturated ones. Many groups have therefore focused on developing molecular cores with π-conjugated building blocks to obtain β values in the range of 0.2−0.6 Å^{-1}.[26,35,40] Recently, single-molecule junctions with highly conjugated, low band gap oligomers have shown efficient long-range charge transport with very small β values ($\leq$0.2 Å^{-1});[13,31,41−43] for example, butadiyne-bridged porphyrin oligomers have β of 0.04 Å^{-1}, suggesting that resonant mechanisms may be operative.[41] Notably, Choi et al. found that the systematic molecular length increase of the conjugated phenylene−imine oligomer core produced a transition from tunneling to resonant transport.[37] The nature of π-conjugation, the magnitude of the band gap, and molecular length play important roles in controlling transport mechanisms.

The choice of the linker connecting the molecular core to the electrodes is equally crucial in determining transport characteristics. A linker can shift the core states close to the metal Fermi energy, thus lowering the tunneling barrier. In addition, linkers can also decrease the contact resistance, so that the intrinsic conductance of the molecular core dominates the m−M−m response. Recent STM break-junction studies[44−46] of alkane chain conductance varying both the electrode material (Au, Pd, Pt) as well as the terminal linker group (dithiol,

(20) Park, H.; Lim, A. K. L.; Alivisatos, A. P.; Park, J.; McEuen, P. L. *Appl. Phys. Lett.* **1999**, *75*, 301–303.
(21) Strachan, D. R.; Smith, D. E.; Johnston, D. E.; Park, T. H.; Therien, M. J.; Bonnell, D. A.; Johnson, A. T. *Appl. Phys. Lett.* **2005**, *86*, 043109.
(22) Venkataraman, L.; Klare, J. E.; Nuckolls, C.; Hybertsen, M. S.; Steigerwald, M. L. *Nature* **2006**, *442*, 904–907.
(23) Seminario, J. M.; De La Cruz, C. E.; Derosa, P. A. *J. Am. Chem. Soc.* **2001**, *123*, 5616–5617.
(24) Li, X. L.; He, J.; Hihath, J.; Xu, B. Q.; Lindsay, S. M.; Tao, N. J. *J. Am. Chem. Soc.* **2006**, *128*, 2135–2141.
(25) Lindsay, S. M.; Ratner, M. A. *Adv. Mater.* **2007**, *19*, 23–31.
(26) Nitzan, A.; Ratner, M. A. *Science* **2003**, *300*, 1384–1389.
(27) Ramachandran, G. K.; Hopson, T. J.; Rawlett, A. M.; Nagahara, L. A.; Primak, A.; Lindsay, S. M. *Science* **2003**, *300*, 1413–1416.
(28) Venkataraman, L.; Klare, J. E.; Tam, I. W.; Nuckolls, C.; Hybertsen, M. S.; Steigerwald, M. L. *Nano Lett.* **2006**, *6*, 458–462.
(29) He, J.; Chen, F.; Li, J.; Sankey, O. F.; Terazono, Y.; Herrero, C.; Gust, D.; Moore, T. A.; Moore, A. L.; Lindsay, S. M. *J. Am. Chem. Soc.* **2005**, *127*, 1384–1385.
(30) Xu, B. Q. Q.; Li, X. L. L.; Xiao, X. Y. Y.; Sakaguchi, H.; Tao, N. J. J. *Nano Lett.* **2005**, *5*, 1491–1495.
(31) Yamada, R.; Kumazawa, H.; Noutoshi, T.; Tanaka, S.; Tada, H. *Nano Lett.* **2008**, *8*, 1237–1240.
(32) Chen, F.; Hihath, J.; Huang, Z. F.; Li, X. L.; Tao, N. J. *Ann. Rev. Phys. Chem.* **2007**, *58*, 535–564.
(33) Haiss, W.; Albrecht, T.; van Zalinge, H.; Higgins, S. J.; Bethell, D.; Hobenreich, H.; Schiffrin, D. J.; Nichols, R. J.; Kuznetsov, A. M.; Zhang, J.; Chi, Q.; Ulstrup, J. *J. Phys. Chem. B* **2007**, *111*, 6703–6712.
(34) Nishikawa, A.; Tobita, J.; Kato, Y.; Fujii, S.; Suzuki, M.; Fujihira, M. *Nanotechnology* **2007**, *18*, 424005.
(35) Adams, D. M.; et al. *J. Phys. Chem. B* **2003**, *107*, 6668–6697.
(36) Chen, F.; Huang, Z. F.; Tao, N. J. *Appl. Phys. Lett.* **2007**, *91*, 162106.
(37) Choi, S. H.; Kim, B.; Frisbie, C. D. *Science* **2008**, *320*, 1482–1486.
(38) Kim, B.; Beebe, J. M.; Jun, Y.; Zhu, X. Y.; Frisbie, C. D. *J. Am. Chem. Soc.* **2006**, *128*, 4970–4971.
(39) Liu, K.; Li, G. R.; Wang, X. H.; Wang, F. S. *J. Phys. Chem. C* **2008**, *112*, 4342–4349.
(40) Salomon, A.; Cahen, D.; Lindsay, S.; Tomfohr, J.; Engelkes, V. B.; Frisbie, C. D. *Adv. Mater.* **2003**, *15*, 1881–1890.
(41) Sedghi, G.; Sawada, K.; Esdaile, L. J.; Hoffmann, M.; Anderson, H. L.; Bethell, D.; Haiss, W.; Higgins, S. J.; Nichols, R. J. *J. Am. Chem. Soc.* **2008**, *130*, 8582–8583.
(42) Chen, I. W. P.; Fu, M. D.; Tseng, W. H.; Chen, C. H.; Chou, C. M.; Luh, T. Y. *Chem. Commun.* **2007**, 3074–3076.
(43) Visoly-Fisher, I.; Daie, K.; Terazono, Y.; Herrero, C.; Fungo, F.; Otero, L.; Durantini, E.; Silber, J. J.; Sereno, L.; Gust, D.; Moore, T. A.; Moore, A. L.; Lindsay, S. M. *Proc. Natl. Acad. Sci.U.S.A.* **2006**, *103*, 8686–8690.
(44) Ko, C. H.; Huang, M. J.; Fu, M. D.; Chen, C. H. *J. Am. Chem. Soc.* **2010**, *132*, 756–764.
(45) Luzhbin, D. A.; Kaun, C. C. *Phys. Rev. B* **2010**, *81*, 035424.
(46) Dalgleish, H.; Kirczenow, G. *Nano Lett.* **2006**, *6*, 1274–1278.

diisothiocyanates) highlight the effect of linker−electrode contact resistance on conductance. While the junctions with Pt electrodes showed ∼3.5 times higher conductance compared to conventional Au electrodes, the dithiol-terminated systems showed roughly an order of magnitude higher conductances relative to the diisothiocyanate-terminated systems.[44] The high affinity of thiolated compounds for gold surfaces, and their synthetic flexibility, have led to their widespread use as linkers to interconnect molecules with electrodes.[26] However, gold−thiol contacts appear to produce only modest interfacial interactions between the molecule and the gold due to weak chemical interactions at the contact.[26,47,48] Hence, the quest for contacts that provide enhanced electronic coupling has become a principal interest in molecular electronics. Molecular conductance studies that probe junctions other than thiol−gold have been reported.[18,23,28,47−56] While the measured conductance of molecules with amine linker groups has less variability than molecules with thiol linkers,[28] the conductance of the amine-terminated molecules is smaller than that determined for analogous compounds that feature thiol linkers, possibly a result of the weaker binding of amines to gold.[28,52] Tivanski et al., however have shown that carbodithioate linkers increase single-molecule conductance through a biphenyl moiety by a factor of 1.4 relative to that provided by thiols.[57] Despite the appeal of the carbodithioate linkers, no further conductance measurements with carbodithioate-functionalized molecules have been reported.

Highly conjugated oligo(phenylene−ethynylene)s (OPEs) have been key structures in molecular electronics.[14,58−64] Most OPE-based molecular junctions have featured thiol linkers and have been assembled in m−M−m junctions by removing an acetyl protecting group, thus enabling the synthesis of π-conjugated oligomers via cross-coupling reactions and preventing free thiols from oxidizing to disulfides. Similar to the acetyl protection of thiols, (trimethylsilyl)ethyl (TMSE) protection makes possible the synthesis of carbodithioate-terminated OPEs via Sonogashira cross-coupling reactions; in situ deprotection enables functionalization of gold nanoparticle surfaces.[65] Thus, it is possible to compare the conductance of m−M−m junctions featuring OPE molecules having both thiol- and carbodithioate-termini.

In a recent study, the conductance of OPE molecular wires of different lengths terminated with amine linkers was explored using STM break junction and CP-AFM measurements.[66] The authors demonstrated a tunneling ($\beta \approx 0.2$ Å^{-1}) to hopping transition ($\beta \approx 0.03$ Å^{-1}) for OPE molecules at slightly longer lengths than considered in this work (*vide infra*). The present work interrogates the extent to which conductance is augmented through OPE molecules terminated with carbodithioate linkers relative to identical structures that are terminated with dithiol linkers. A surprising result is that carbodithioate-terminated OPE molecules show small β (∼0.05 Å^{-1}) values, even for modest molecular length scales. Whether this value is maintained or lowered further upon increasing the molecular length will be a focus of future studies. The theoretical analysis[66] of the amine-terminated OPE conductance data, which did not take the full electronic structure of the molecule into account, estimates a barrier for charge injection which can be correlated with the energies of the frontier orbitals (HOMO/LUMO). We employ a more detailed model (*vide infra*) that fully takes into account molecular electronic structure. This approach allows us to distinguish between hole (filled molecular orbitals)- or electron (empty molecular orbital)-mediated charge transport. Furthermore, we show that the barrier for charge transport cannot, in general, be determined from the knowledge of the molecular frontier orbitals energies (or their separation from the Fermi level) alone. It is essential to analyze whether the coupling between the frontier orbitals and the electrode is sufficiently strong that significant charge transport is mediated by these MOs.

Over the past decade, nonequilibrium Green's function (NEGF) methods have become particularly useful in molecule-mediated transport studies.[10,67−72] The NEGF formalism for charge transport,[67] combined with *ab initio* density functional theory (DFT) for electronic-structure calculations, forms the self-consistent DFT-NEGF approach to compute the coherent transport properties for modeled m−M−m systems.[68,69] For example, Sankey and Tomfohr calculated molecular conductances in agreement with experiments for a number of organic molecules.[10] This approach was extended to analyze inelastic transport,[70] and applied to conjugated oligo(phenylenevinylene)s (OPVs), OPEs, and alkane bridges connected by thiol linkers to gold electrodes.[71] The influence of conformational sampling on transport was recently investigated using NEGF calculations

(47) Li, Z. Y.; Kosov, D. S. *J. Phys. Chem. B* **2006**, *110*, 19116–19120.
(48) Tulevski, G. S.; Myers, M. B.; Hybertsen, M. S.; Steigerwald, M. L.; Nuckolls, C. *Science* **2005**, *309*, 591–594.
(49) Kushmerick, J. G.; Naciri, J.; Yang, J. C.; Shashidhar, R. *Nano Lett.* **2003**, *3*, 897–900.
(50) Yaliraki, S. N.; Kemp, M.; Ratner, M. A. *J. Am. Chem. Soc.* **1999**, *121*, 3428–3434.
(51) Beebe, J. M.; Engelkes, V. B.; Miller, L. L.; Frisbie, C. D. *J. Am. Chem. Soc.* **2002**, *124*, 11268–11269.
(52) Chen, F.; Li, X. L.; Hihath, J.; Huang, Z. F.; Tao, N. J. *J. Am. Chem. Soc.* **2006**, *128*, 15874–15881.
(53) Millar, D.; Venkataraman, L.; Doerrer, L. H. *J. Phys. Chem. C* **2007**, *111*, 17635–17639.
(54) Patrone, L.; Palacin, S.; Bourgoin, J. P. *Appl. Surf. Sci.* **2003**, *212*, 446–451.
(55) Patrone, L.; Palacin, S.; Charlier, J.; Armand, F.; Bourgoin, J. P.; Tang, H.; Gauthier, S. *Phys. Rev. Lett.* **2003**, *91*, 096802.
(56) Yasuda, S.; Yoshida, S.; Sasaki, J.; Okutsu, Y.; Nakamura, T.; Taninaka, A.; Takeuchi, O.; Shigekawa, H. *J. Am. Chem. Soc.* **2006**, *128*, 7746–7747.
(57) Tivanski, A. V.; He, Y. F.; Borguet, E.; Liu, H. Y.; Walker, G. C.; Waldeck, D. H. *J. Phys. Chem. B* **2005**, *109*, 5398–5402.
(58) Chen, J.; Reed, M. A.; Rawlett, A. M.; Tour, J. M. *Science* **1999**, *286*, 1550–1552.
(59) Cai, L. T.; Skulason, H.; Kushmerick, J. G.; Pollack, S. K.; Naciri, J.; Shashidhar, R.; Allara, D. L.; Mallouk, T. E.; Mayer, T. S. *J. Phys. Chem. B* **2004**, *108*, 2827–2832.
(60) Chen, J.; Wang, W.; Reed, M. A.; Rawlett, A. M.; Price, D. W.; Tour, J. M. *Appl. Phys. Lett.* **2000**, *77*, 1224–1226.
(61) Selzer, Y.; Cai, L.; Cabassi, M. A.; Yao, Y.; Tour, J. M.; Mayer, T. S.; Allara, D. L. *Nano Lett.* **2005**, *5*, 61–65.
(62) Tour, J. M.; Rawlett, A. M.; Kozaki, M.; Yao, Y. X.; Jagessar, R. C.; Dirk, S. M.; Price, D. W.; Reed, M. A.; Zhou, C. W.; Chen, J.; Wang, W. Y.; Campbell, I. *Chem.−Eur. J.* **2001**, *7*, 5118–5134.
(63) Walzer, K.; Marx, E.; Greenham, N. C.; Less, R. J.; Raithby, P. R.; Stokbro, K. *J. Am. Chem. Soc.* **2004**, *126*, 1229–1234.
(64) Xiao, X. Y.; Nagahara, L. A.; Rawlett, A. M.; Tao, N. J. *J. Am. Chem. Soc.* **2005**, *127*, 9235–9240.
(65) Park, T. H.; Therien, M. J. *Org. Lett.* **2007**, *9*, 2779–2782.
(66) Lu, Q.; Liu, K.; Zhang, H.; Du, Z.; Wang, X.; Wang, F. *ACS Nano* **2009**, *3*, 3861–3868.
(67) Datta, S. *Quantum Transport: Atom to Transistor*; Cambridge University Press: New York, 2005.
(68) Xue, Y. Q.; Datta, S.; Ratner, M. A. *Chem. Phys.* **2002**, *281*, 151–170.
(69) Brandbyge, M.; Mozos, J. L.; Ordejon, P.; Taylor, J.; Stokbro, K. *Phys. Rev. B* **2002**, *65*, 165401.
(70) Troisi, A.; Ratner, M. A. *Phys. Rev. B* **2005**, *72*, 033408.
(71) Paulsson, M.; Frederiksen, T.; Brandbyge, M. *Nano Lett.* **2006**, *6*, 258–262.
(72) Andrews, D. Q.; Van Duyne, R. P.; Ratner, M. A. *Nano Lett.* **2008**, *8*, 1120–1126.

on benzenedithiol, benzenediamine and biphenyldithiol[72−75] In the biphenyldithiol studies, DFT-NEGF calculations were performed on three molecule-electrode geometries extracted from MD simulations.[73−75] In the benzenedithiol and benzenediamine studies, conductance calculations on hundreds of molecule−electrode geometries, and four different electrode separation distances were performed using a Hückel Hamiltonian.[72]

The self-consistent DFT-NEGF approach calculates the interaction between metal electrodes and the molecule from first principles. Each electrode is usually modeled as a finite set of less than 50 lattice atoms. There are some issues regarding the application of these methods to m−M−m systems, most of them arising from the choice of the exchange correlational functional (XCF).[76−81] Compounding the standard limitations of DFT, describing nonequilibrium processes with an equilibrium XCF can lead to an overestimate of currents in molecules that weakly couple to electrodes (see Supporting Information, SI). Li and Kosov[47] studied the enhancement of molecular conductance through a biphenyl core structure when carbodithioate functional groups were used in place of thiols. They used the DFT-NEGF approach in the strong molecule-electrode coupling limit. Strong coupling modifies the molecular eigenstates/eigenenergies and strongly mixes molecule and electrode eigenstates. This approach is implemented in their analysis by considering an extended molecule, i.e. including Au atoms at the interface as part of the molecule.

However, it is not clear that the gold−thiol linker coupling is in fact strong. Rather, it was proposed that the thiol−Au interactions are structural rather than chemical, suggesting that there is negligible charge transfer between the thiol and the gold.[48] As such, interactions with the electrodes are unlikely to significantly modify the energy and electron occupation of sulfur 3p orbitals.[48] This was also noted by Li and Kosov.[47] A comprehensive DFT study[82,83] of alkane, aromatic, and alkyne molecules attached by thiol linkers to Au clusters showed (for neutral systems): (a) negligible charge transfer between sulfur and gold atoms, and (b) weak mixing of the molecule−metal states. Thus, while we cannot eliminate the possibility of strong electrode−molecule couplings in these systems, it is reasonable to explore the conductivity of the OPE systems in the weak electrode−molecule coupling regime.[84] In this limit, the influence of the electrode is to broaden the molecular eigenstates weakly. The eigenstates do not lose either their symmetry or their qualitative charge distribution characteristics compared to the isolated molecule. As described below, our model parametrizes the conductance calculations so that we can analyze the dependence of the absolute and relative conductance, contact resistance, and distance-dependent conductance decay on the relative location of the metal Fermi energy with respect to the molecular eigenstate energies and the electrode−molecule coupling. Moreover, in the weak coupling limit, the conductance can be analyzed in terms of the isolated molecule properties. Insights gained regarding molecular contributions are independent of the electrode type and are transferable to other weak coupling m−M−m systems.

Chart 1. Structure of α,ω-Dithiol-Terminated (**T1**, **T2**, and **T3**) and α,ω-Bis-carbodithioate-Terminated π-Conjugated Molecules (**C1**, **C2**, and **C3**)

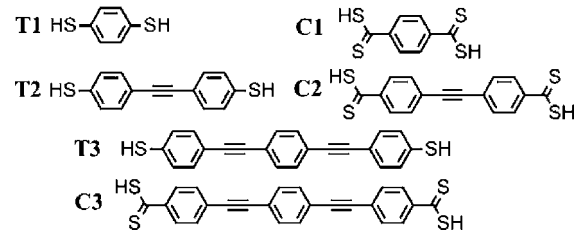

We have experimentally measured the conductance of thiol and carbodithioate-terminated OPEs using STM break-junctions, and investigated the length dependence of the molecular conductance with thiol and carbodithioate linkers. We also performed nonequilibrium Green's function calculations to evaluate the effect of the linker on charge transport. Experimental results show that the carbodithioate linkers not only increase the molecular conductance compared to their thiol counterparts (except for the shortest C1 (Chart 1) molecule) but also provide a quasi-linear length dependence of conductivity for the OPE molecular wires. Our theoretical analysis dissects the contributions of individual molecular orbitals to the conductivity and shows that the carbodithioate linkers facilitate electronic coupling between the OPE molecules and the electrodes as well as provide lower contact resistance compared to the thiol linkers.

Experimental Section

Materials. 1,4-Benzenedithiol (**T1**) was purchased from Alfa Aesar and used as received. The synthesis and characterization of 2-(trimetylsilyl)ethyl ester derivative of **C1** are found in the SI. The acetyl-protected versions of dithiol **T2** and **T3**[62,85] and the TMSE esters of **C2** and **C3**[65] were synthesized according to literature procedures.

Self-Assembled Monolayer (SAM) Preparation. A gold bead was prepared using Clavilier's method[86] and cleaned by piranha solution (H_2SO_4/H_2O_2 = 3:1) and hydrogen flame annealed in air. **(Caution! Piranha solution is a very strong oxidizing reagent and can be dangerous to handle. Protective equipment including gloves and goggles should be used at all times.)** After cooling, the gold bead was immersed into a THF solution containing 100 μM of the target molecule (Chart 1) for 15−30 min to prepare a self-assembled monolayer (SAM). The adsorbate solutions were prepared by deprotection of the precursor molecules (SI) and used immediately. The sample was rinsed by THF and dried under a

(73) Jang, S. S.; Jang, Y. H.; Kim, Y. H.; Goddard, W. A.; Choi, J. W.; Heath, J. R.; Laursen, B. W.; Flood, A. H.; Stoddart, J. F.; Norgaard, K.; Bjornholm, T. *J. Am. Chem. Soc.* **2005**, *127*, 14804–14816.
(74) Jang, S. S.; Jang, Y. H.; Kim, Y. H.; Goddard, W. A.; Flood, A. H.; Laursen, B. W.; Tseng, H. R.; Stoddart, J. F.; Jeppesen, J. O.; Choi, J. W.; Steuerman, D. W.; DeIonno, E.; Heath, J. R. *J. Am. Chem. Soc.* **2005**, *127*, 1563–1575.
(75) Kim, Y. H.; Jang, S. S.; Goddard, W. A. *J. Chem. Phys.* **2005**, *122*, 244703.
(76) Evers, F.; Weigend, F.; Koentopp, M. *Phys. Rev. B* **2004**, *69*, 23541.
(77) Koentopp, M.; Chang, C.; Burke, K.; Car, R. *J. Phys.: Condens. Matter* **2008**, *20*, 083203.
(78) Ke, S. H.; Baranger, H. U.; Yang, W. T. *J. Chem. Phys.* **2007**, *126*, 201102.
(79) Toher, C.; Filippetti, A.; Sanvito, S.; Burke, K. *Phys. Rev. Lett.* **2005**, *95*, 146402.
(80) Reimers, J. R.; Cai, Z. L.; Bilic, A.; Hush, N. S.; Reimers, J. R.; Picconatto, C. A.; Ellenbogen, J. C.; Shashidhar, R. *Ann. N.Y. Acad. Sci.* **2003**, *1006*, 235−251.
(81) Koentopp, M.; Burke, K.; Evers, F. *Phys. Rev. B* **2006**, *73*, 121403.
(82) Basch, H.; Ratner, M. A. *J. Chem. Phys.* **2003**, *119*, 11926–11942.
(83) Basch, H.; Ratner, M. A. *J. Chem. Phys.* **2003**, *119*, 11943–11950.
(84) Yoshizawa, K.; Tada, T.; Staykov, A. *J. Am. Chem. Soc.* **2008**, *130*, 9406–9413.
(85) Hsung, R. P.; Babcock, J. R.; Chidsey, C. E. D.; Sita, L. R. *Tetrahedron Lett.* **1995**, *36*, 4525–4528.
(86) Clavilier, J.; Faure, R.; Guinet, G.; Durand, R. *J. Electroanal. Chem.* **1980**, *107*, 205–209.

Figure 1. Schematic for the separation of the electrode−molecule−electrode system for NEGF calculations into the three subsystems: The device region (center) with the molecule and thiol/carbodithioate and linkers (shown are **T2** and **C2** from Chart 1); and the left and right featureless electrodes (contacts) characterized purely in terms of the chemical potentials μ_L/μ_R. ε_F is the Fermi energy, q is the electron charge and V is the applied potential bias which is assumed to drop symmetrically across the two electrodes. Note that the electronic structural calculations considered uncharged OPE molecules.

nitrogen stream, then put into the liquid cell of a PicoPlus Scanning Probe Microscope (Molecular Imaging, Tempe, AZ) system and covered with toluene.

Conductivity Measurements. A fresh cut gold tip (0.25 mm, 99.999%, Alfa Aesar) was used to image a SAM-covered gold bead surface immersed in toluene; the quality of the tip was judged by the ability to resolve gold atomic steps in STM images. The tip was then brought into contact with the surface and withdrawn at a rate of ∼20 nm/s, while measuring current. This process was repeated thousands of times and a current−distance curve was recorded each time. When a molecule bridges the tip−substrate gap, the current shows step-like features instead of a simple exponential decay. Statistical analysis of the curves showing quantized conductance peaks reflects the conductance of single molecules.

Theoretical Methods. We calculated conductances for the thiol- and carbodithioate-terminated OPE structures, using nonequilibrium Green's function (NEGF) methods[67] on DFT-optimized structures. As opposed to the conventional DFT-NEGF methods, which include parts of the electrode in the DFT calculation, we worked in the weak coupling limit, using DFT to calculate the geometry of the isolated molecule (core plus linker) and used molecular orbital information (as calculated using INDO/s) as input to NEGF calculations. The effect of the electrodes is described with a molecule-electrode coupling parameter that broadens the density of states of the isolated molecule. Charge is injected into the molecule at the electrode Fermi energy.

1. Electronic Structure Calculations. Three carbodithioate-terminated systems (CTS) and three dithiol-terminated systems (DTS; Chart 1) were built, and the geometry was optimized using DFT and a B3LYP exchange correlation functional with a 6-31G* basis set, in Gaussian 03.[87] The electronic structure of these geometry optimized structures was calculated using an INDO/s Hamiltonian[88] as implemented in the CNDO code,[89] and the molecular orbitals were used as input to the NEGF analysis of transport properties. The semiempirical INDO/s approach provides a useful balance between cost and performance.[88,90,91] Specifically, for this investigation, we find the character of MOs and trends in their relative energies within each molecule and across different molecules to be the same qualitatively for INDO/s and DFT calculations, as shown Figure S3 (SI).

2. NEGF Calculations. In the NEGF approach[67] the electrode−molecule−electrode system is partitioned into three subsystems (Figure 1): a device region (the isolated molecule) and two structureless electrodes. The Green's function describes the molecule and its interactions with the electrodes:

$$\boldsymbol{G}(E) = \frac{1}{(E\mathbf{I} - \mathbf{H} - \Sigma_L - \Sigma_R)} \tag{1}$$

H is the Hamiltonian and **I** is the identity matrix of the isolated molecule. The self-energies Σ describe the broadening and shifts in molecular energies induced by the right (R) and left (L) electrodes. The transmission coefficient sums over all pathways for charge transport at energy E from one electrode to the other:

$$T(E) = Tr[\boldsymbol{\Gamma}_L \boldsymbol{G} \boldsymbol{\Gamma}_R \boldsymbol{G}^+] \tag{2}$$

The broadening matrix: $\Gamma = i\,[\Sigma - \Sigma^+]$ is proportional to the imaginary part of the self-energy. In conventional DFT-NEGF schemes, the broadening matrices and Green's functions are computed for an explicit m−M−m system.[10,47,68] Since we work in the weak-electrode molecule coupling limit, we use the broadening matrix as a parameter represented in our calculations in the basis of atomic orbitals. The molecule is assumed to contact the metal electrodes only via the sulfur atoms, i.e. only orbitals of the sulfur atoms are broadened, and the couplings among atomic orbitals are not affected by the contacts. The elements of the broadening matrix, are:

$$\begin{aligned} \Gamma_{ii} &= \gamma \text{ for all sulfur atoms atomic orbitals} \\ \Gamma_{ii} &= 0 \text{ otherwise} \\ \Gamma_{ij} &= 0 \text{ for } i \neq j \end{aligned} \tag{3}$$

Here, i and j are atomic orbital indices and γ is the sulfur−gold coupling parameter. The real parts of the self-energies are assumed to be small compared to the energy separation of the sulfur atomic orbitals (diagonal elements of the Fock matrix) from all other molecular orbitals. The magnitude of the sulfur−gold coupling (γ) was chosen to be small (relative to the separation among diagonal elements of the Fock matrix). The transmission coefficient (or current) can be partitioned into contributions from individual molecular orbitals. The Green's function in the basis of molecular eigenstates is:

$$G(E) = \frac{1}{\left[E\mathbf{I} - \mathbf{H}' + \frac{i}{2}(\boldsymbol{\Gamma}'_L + \boldsymbol{\Gamma}'_R)\right]}; \quad \mathbf{H}' = \mathbf{U}^+\mathbf{H}\mathbf{U}; \boldsymbol{\Gamma}'_{L/R} = \mathbf{U}^+\boldsymbol{\Gamma}_{L/R}\mathbf{U} \tag{4}$$

U diagonalizes the Fock matrix H. The current is given by the Landauer expression:

$$I(V) = \frac{q}{h}\int T(E)[f_L(E) - f_R(E)]\mathrm{d}E \tag{5}$$

The Fermi function defines the electron occupancy for each electrode:

$$f_{L/R}(E) = \frac{1}{1 + \exp[(E - \mu_{L/R})/k_BT]} \tag{6}$$

Here $\mu_{L/R}$ are the chemical potentials of the left/right electrodes:

$$\mu_L = E_F + qV/2; \mu_R = E_F - qV/2 \tag{7}$$

The Fermi energy E_F is the same for both electrodes if they are made of the same metal, and V is an external potential bias (taken in the range of 0−100 mV in the calculations here). The potential drop is assumed to be symmetric across the electrodes. The small biases applied here are not expected to cause significant changes in molecular geometry or energies, and no potential drop is assumed across the molecule. Our calculations are expected to capture

(87) Frisch, M. J.; et al. *Gaussian 03*, Revision D.02; Gaussian Inc: Wallingford, CT, 2004.
(88) Ridley, J.; Zerner, M. *Theor. Chim. Acta* **1973**, *32*, 111–134.
(89) Zeng, J.; Hush, N. S.; Reimers, J. R. *J. Am. Chem. Soc.* **1996**, *118*, 2059–2068.
(90) Hutchison, G. R.; Ratner, M. A.; Marks, T. J. *J. Phys. Chem. A* **2002**, *106*, 10596–10605.
(91) Voityuk, A. A. *Chem. Phys. Lett.* **2006**, *427*, 177–180.

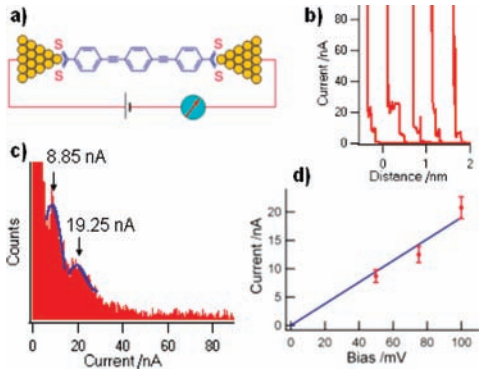

Figure 2. (a) Scheme for single-molecule (**C3**) conductance measurements. (b) Example of current−distance curves recorded with **C3** in the junction at 50 mV bias. (c) Histogram analysis of **C3** conductance constructed from ~150 *I*−*S* curves. (d) Conductance of **C3** is determined by fitting the measurements at different bias values.

Table 1. Conductance Measurement of **T1**−**T3** and **C1**−**C3**

	conductance/G_0[a]	conductance/nS	resistance/MΩ
T1	$8.3\ (\pm 0.7) \times 10^{-3}$	639 ± 54	1.6 ± 0.13
T2	$2.6\ (\pm 0.4) \times 10^{-4}$	20 ± 3	50 ± 7.6
T3	$1.3\ (\pm 0.3) \times 10^{-4}$	10 ± 2	100 ± 25
C1	$4.8\ (\pm 0.5) \times 10^{-3}$	367 ± 39	2.7 ± 0.3
C2	$3.2\ (\pm 1.1) \times 10^{-3}$	246 ± 54	4.1 ± 0.9
C3	$2.5\ (\pm 0.3) \times 10^{-3}$	193 ± 23	5.2 ± 0.6

[a] $G_0 = 2e^2/h = 77\ \mu S = 13\ k\Omega$.

relative trends, and we analyze the relationship between molecular structure and conductance trends for CTS and DTS.

Results and Discussion

1. Molecular Conductance Measurements. The single-molecule conductance of π-conjugated organic molecules with thiol or carbodithioate linkers (Chart 1) was measured via the STM break-junction method[18] (Figure 2a). Typical current−distance curves, showing clear conductance steps, are shown for **C3** in Figure 2b. The histogram analysis (Figure 2c) shows well-defined peaks in which the magnitude of the second current peak is about twice that of the first. This suggests that the first current peak corresponds to single-molecule junctions, while the second peak corresponds to the junction formed from pairs of molecules.[18] The conductances for all six systems in Chart 1 were obtained by linear fitting of the current peaks acquired at multiple biases and are listed in Table 1. Out of the six molecules studied here, two (**T1** and **T3**) have been studied previously using the STM break-junction method by Tao and co-workers. Our conductance values for **T1** and **T3** are comparable to those obtained previously (**T1**, 833 ± 90 nS;[92] **T3**, ~13 nS).[64]

Table 1 shows that with the exception of benzene-based **C1** and **T1**, the carbodithioate linker enhances the conductance of OPE molecules by an order of magnitude relative to corresponding phenylene−ethynylenes that possess thiol linkers.

The conductance of benzenedithiol (**T1**) does not follow the decay trend of **T2** and **T3** (Figure 3) and is roughly two times higher than **C1**. The **T1** system has proved notoriously difficult to characterize using break junction experiments, exhibiting a wide range of conductance values ($0.01G_0$−$0.1G_0$).[16,92−95] It

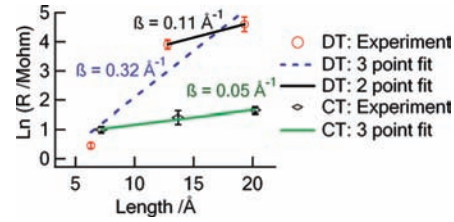

Figure 3. Natural logarithmic plot of the resistance of dithiols (**T1**−**T3**) and carbodithioates (**C1**−**C3**) versus molecular length. The β values are calculated through the semilogarithmic plot of resistance and molecule length based on $R = R_0 \exp(\beta L)$.

has been proposed[10,96] that this variation in conductance arises due to multiple contact configurations of the benzedithiol molecule with the electrodes. A careful reanalysis of break junction experimental data was performed on alkanethiol systems of varying length to reveal a second series of current peaks corresponding to a lower conductance value.[96] On the basis of simulation studies[10] the observed variation in conductance was attributed to two different contact configurations of the sulfur atom with the gold surface; data obtained from additional simulations showed further that this effect diminishes with molecular length.

Comparing the conductances measured for **C2**−**C3** and **T2**−**T3**, it is clear that the carbodithioate linker improves the conductance of OPE molecules by over an order of magnitude and highlights the importance of optimizing the molecule−electrode junction to enhance molecular conductivity and access the intrinsic core conductivity. The order of magnitude improvement in the conductivity of OPEs observed by changing to the molecular termini from thiol to carbodithioate is significantly greater than the 1.4-fold conductance enhancement observed in experiments involving biphenyl junctions.[57]

The β value determined from the length dependence of **T1**−**T3** resistances is 0.32 ± 0.10 Å^{-1} (blue dashed line, Figure 3). The data, however, deviate significantly from the fitting line, because of the atypical behavior of **T1.** We exclude the conductance of **T1** from further analysis due to the uncertainties in measuring the conductances of short molecules such as **T1** using break-junction methods (vide supra). Omitting the **T1** resistance in this analysis suggests $\beta = 0.11 \pm 0.06$ Å^{-1} (black line, Figure 3), a value much lower than the theoretical estimate of 0.27 Å^{-1} determined for dithiol OPE wires,[10] and rather close to tunneling decay constants measured for other α,ω-dithiol-terminated π-conjugated molecules using the STM break-junction methods.[29,31,42]

Carbodithioate-terminated **C1**−**C3**, on the other hand, show a β of 0.05 ± 0.01 Å^{-1} (green line, Figure 3), a value lower than their dithiol analogues and other dithiol π-conjugated oligomers.[29,31,42] A comparably low β value derived from single-molecule conductance measurements has only been realized with dithiol-terminated butadiyne-bridged porphyrin oligomers ($\beta = 0.04 \pm 0.006$ Å^{-1}).[41] In these systems, the extension of π-conjugation reduces the gap between the donor and the bridge states (in butadiyne-bridged D−B−A systems) or between the electrode Fermi level and the bridge states (in these m−M−m junctions). In Figure S3 (SI), we report the calculated

(92) Xiao, X. Y.; Xu, B. Q.; Tao, N. J. *Nano Lett.* **2004**, *4*, 267–271.
(93) Ulrich, J.; Esrail, D.; Pontius, W.; Venkataraman, L.; Millar, D.; Doerrer, L. H. *J. Phys. Chem. B* **2006**, *110*, 2462–2466.
(94) Ghosh, S.; Halimun, H.; Mahapatro, A. K.; Choi, J.; Lodha, S.; Janes, D. *Appl. Phys. Lett.* **2005**, *87*, 233509/1–233509/3.
(95) Tsutsui, M.; Teramae, Y.; Kurokawa, S.; Sakai, A. *Appl. Phys. Lett.* **2006**, *89*, 163111/1–163111/3.
(96) He, J.; Sankey, O.; Lee, M.; Tao, N. J.; Li, X. L.; Lindsay, S. *Faraday Discuss.* **2006**, *131*, 145–154.

HOMO−LUMO gaps for both the **C1**−**C3** and **T1**−**T3** systems, calculated using DFT as well as INDO/s methods. The computed CTS HOMO−LUMO gaps are lower than those evinced for DTS, for identical phenylene−ethynylene cores.[65] However, the CTS HOMO−LUMO gaps are also much larger than those previously reported for the butadiyne-bridged porphyrin oligomers (1.8−2.1 eV); thus, in order for the CTS to exhibit a low β value comparable to that determined for butadiyne-bridged porphyrin oligomers in m−M−m junctions, the carbodithioate-mediated coupling strength between the contacts and the bridge states must exceed that for thiol-mediated coupling. These results thus show the critical importance of the nature of the molecule-to-metal contact upon bridge electronic structure, and suggest that the OPE core is much more conductive than previously thought.

2. Calculations of Molecular Conductances. The computations described above were performed to explore the origins of improved conductance in CTS and its weaker dependence on OPE length relative to the analogous thiol-terminated systems. In the following sections, we first analyze the conductance of CTS and DTS in the limits of both deep tunneling and resonant transport regimes. Connections to the experimental results are then made in calculations which do not *a priori* assume any particular transport mechanism.

2.1. Tunneling Currents. In the tunneling regime, the electrode Fermi level lies in the gap between filled and empty molecular orbitals. The Fermi level is far enough (energetically) from the HOMO or LUMO that the dominat contribution to the current (eq 5) arises from transmission near the Fermi energy. The tunneling current is given by:

$$I^{\mathrm{Tun}}(V) = \left(\frac{q^2V}{h}\right) \times T(E = E_{\mathrm{F}}) \tag{8a}$$

with

$$T(E = E_{\mathrm{F}}) = \sum_m SF_m^{\mathrm{Tun}} \tag{8b}$$

and

$$SF_m = \sum_n \frac{\Gamma^{\mathrm{L}}_{mn}\Gamma^{\mathrm{R}}_{nm}}{(E_{\mathrm{F}} - E_m)(E_{\mathrm{F}} - E_n)} \tag{8c}$$

where n and m are MO indices and the sums run over all MOs. Here, the transmission coefficient in eq 2 (and the current) were decomposed into contributions from specific molecular orbitals m given by the scoring factor SF_m. Equation 8c uses $E_{\mathrm{F}} - E_m + 0.5i(\Gamma^{\mathrm{L}}_{mm} + \Gamma^{\mathrm{R}}_{mm}) \approx E_{\mathrm{F}} - E_m$. When $m = n$, the score represents a pure contribution from orbital m with broadening matrix elements Γ^{L}_{mm} and Γ^{R}_{mm}, which are positive in nature. When $m \neq n$, the score represents a contribution arising from the electrode induced coupling of orbital m to orbital n. These contributions can be positive or negative, depending on the sign of the broadening matrix elements. We assumed $E_{\mathrm{F}} = -5.1$ eV (typical for Au) and a sulfur−gold coupling parameter $\gamma = 0.1$ (eq 3) for all six systems (**C1**−**C3** and **T1**−**T3**). While γ is the same for sulfur atomic orbitals in all systems (CTS and DTS), the differences in mixing of each molecule's sulfur atomic orbitals with the molecular core leads to completely different couplings between the molecule and the electrodes. The computed current−voltage curves are linear over the range of the applied bias (0−100 mV). The conductance (or resistance) for each system was computed from the slope of the current−voltage curves. Table 2 shows that the calculated resistances for DTS are about an order of magnitude larger than for CTS. The computed β values are comparable for both systems (0.42 Å^{-1} for CTS and 0.43 Å^{-1} for DTS), while the evaluated contact resistance, R_0, for CTS (**C1**−**C3**, 1.94 MΩ) is nearly an order of magnitude smaller than that for DTS (**T2** and **T3**, 12.02 MΩ), providing evidence that improving the coupling at the contacts enhances the conductivity of CTS relative to the corresponding DTS.

Table 2. Calculated Resistance Values for Tunneling Currents in CT and DT Systems[a]

system	R (MΩ)	system	R (MΩ)
C1	3.2613×10^3	**T1**	2.8474×10^4
C2	3.7858×10^4	**T2**	5.6488×10^5
C3	9.8815×10^5	**T3**	1.04×10^7

[a] $E_{\mathrm{F}} = -5.1$ eV and $\gamma = 0.1$ eV.

Figure 4 plots the scoring factor as a function of MO energy. While the barrier for hole injection is lower than that for electron injection in both systems, the electron current through empty states cannot be disregarded (relative to the hole current) for CTS. Both contribute comparably in CTS while hole transport dominates for DTS. Visualization of MO contributions (parts A and B Figure 5) show that the strongest contribution to the current comes from delocalized MOs with large amplitudes on the terminal sulfurs (not necessarily the HOMO or LUMO). For these molecules, the frontier orbitals need not dominate the conductance. Further, even if the frontier orbitals couple strongly to the electrodes, they may have low scoring factors because contact-induced couplings to neighboring orbitals with phase opposite to those of the frontier orbitals can lead to destructive interferences. In eq 8c the pure contributions for an orbital ($m = n$) can cancel with a cross term ($m \neq n$) if orbitals m and n are energetically close and have opposite phases. As an example, Figure 5C shows two neighboring high-lying filled **C1** orbitals (HOMO−2 and HOMO−1), which are strongly coupled to the electrodes as seen from the large amplitudes on the terminal sulfurs. This MO pair has nearly equal energy. Yet, one MO has terminal group amplitudes of the same sign; the other MO has terminal group amplitudes of opposite sign. Thus, these two nearly degenerate MOs interfere destructively (see eq 8c), leading to nearly canceling scoring factors highlighted in Figure 4. To see this more clearly, consider the three leading terms in the scoring factor (eq 8c) for the C1 HOMO−1:

$$SF_{\mathrm{HOMO-1}} = \frac{\Gamma^{\mathrm{L}}_{\mathrm{HOMO-1,HOMO}}\Gamma^{\mathrm{R}}_{\mathrm{HOMO,\,HOMO-1}}}{(E_{\mathrm{F}} - E_{\mathrm{HOMO-1}})(E_{\mathrm{F}} - E_{\mathrm{HOMO}})} + \frac{\Gamma^{\mathrm{L}}_{\mathrm{HOMO-1,HOMO-1}}\Gamma^{\mathrm{R}}_{\mathrm{HOMO-1,HOMO-1}}}{(E_{\mathrm{F}} - E_{\mathrm{HOMO-1}})^2} + \frac{\Gamma^{\mathrm{L}}_{\mathrm{HOMO-1,HOMO-2}}\Gamma^{\mathrm{R}}_{\mathrm{HOMO-2,HOMO-1}}}{(E_{\mathrm{F}} - E_{\mathrm{HOMO-1}})(E_{\mathrm{F}} - E_{\mathrm{HOMO-2}})}$$

The denominators of all three terms are virtually identical, since energetic differences between the HOMO, HOMO−1, and HOMO−2 are negligible compared to their separation from the Fermi level (see Figure 4A). The magnitude and sign of the three terms are then decided by the numerator Γ^{L}_{mn} and Γ^{R}_{mn} terms, which represent the coupling of orbital m with orbital n induced by their mutual coupling to the left and right contacts, respectively; these are directly proportional to the product of MO amplitudes on the terminal sulfurs. Since the C1 HOMO−1

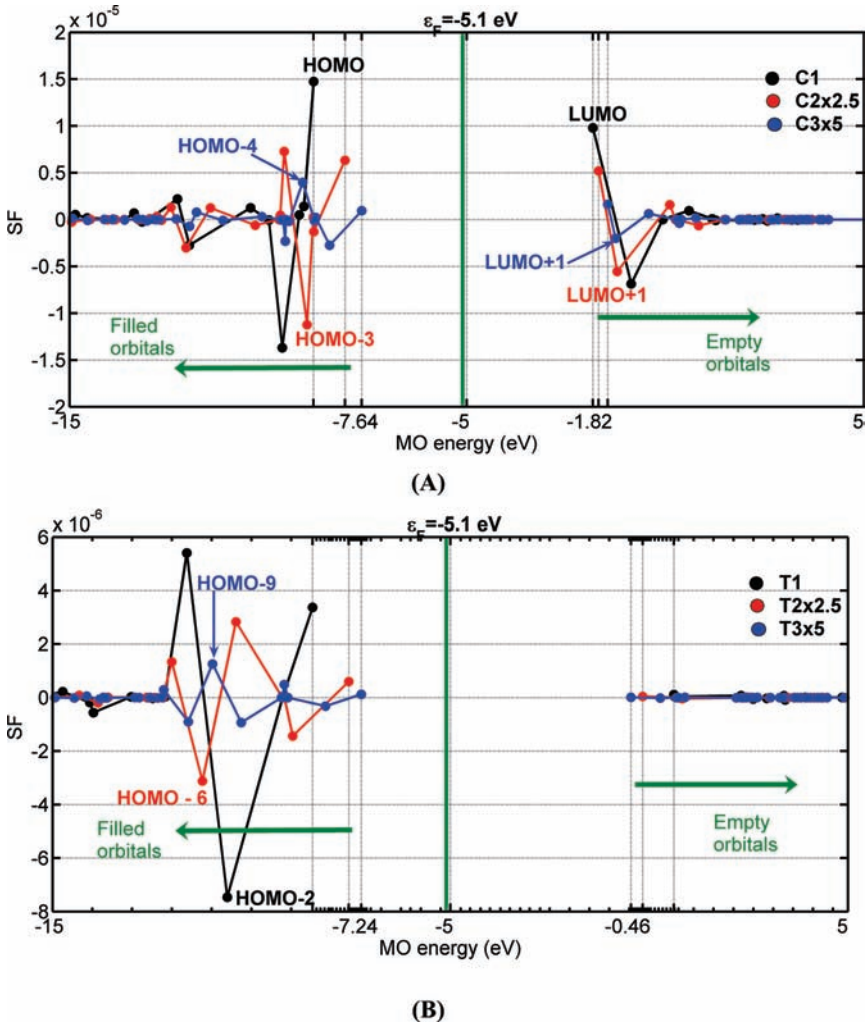

Figure 4. Plots of the scoring factors (eq 8a) for each molecular orbital vs MO energies in the tunneling transport limit wherein the Fermi level is located deep in the HOMO−LUMO gap. The Fermi level and MO energies are plotted with respect to a common vacuum level ($E_{vac} = 0$ eV). The value chosen for the Fermi level energy matches reported values of the gold workfunction (5.1 eV) from the literature. (A) CTS and (B) DTS. For both CT and DT systems, the orbitals with the strongest contributions are labeled. These orbitals are also visually depicted in A and B of Figure 5.

and HOMO−2 orbitals have much larger amplitudes on the terminal sulfurs (Figure 5) than on the C1 HOMO, the second and third terms give the strongest contributions. Further, from Figure 5C, we can infer that the product of MO amplitudes on the terminal sulfurs for the HOMO and HOMO−1 would lead to nearly equal magnitudes but opposite signs for the second and third terms. Thus, a cancellation of the dominant contributions leads to a weak scoring factor for HOMO−1. Parts A and B of Figure 5 show MOs giving the strongest conductance contributions for CTS and DTS respectively. Contact-induced couplings (cross terms in eq 8a) further enable these orbitals to boost the contribution of energetically close neighboring orbitals (via constructive interference), which are more weakly coupled to the electrodes.

Figure 4 shows that the contribution of the HOMO to the tunneling current in CTS is much larger than in DTS, despite the higher barrier for hole injection in CTS. Since the contribution to the tunneling current from a single MO with energy E is proportional to $\Gamma^L\Gamma^R/ [E_F - E]^2$, the broadening matrix elements Γ^L and Γ^R for the CTS HOMO are bigger than those for the analogous DT constructs. In contrast to thiol, the carbodithioate unit is delocalized; for CTS, the combination of π conjugation and an additional terminal sulfur, promotes a π-mediated coupling pathway to the Au surface. The contribution of this π pathway to the current is much larger than that which derives from a pathway involving a single thiol sulfur. We have calculated tunneling currents in CTS for hypothetical cases where the linkers are coupled to the contacts at either end through both carbodithioate sulfurs by setting the coupling of one of the terminal sulfurs on both sides to zero in eq 3. Treating the carbodithioate moiety for the purpose of computation as a linker where one sulfur features a single bond to the terminal carbon while the other features a full C−S double bond (Table 3), shows that the smallest resistance path is mediated by the double-bonded sulfurs. These data underscore the importance of π conjugation in fixing the magnitude of linker−electrode coupling. The couplings to the contacts through double-bonded sulfurs (Figure S2 (SI), Table 3) at both ends give currents that are 2 orders of magnitude larger than those obtained by coupling through single-bonded sulfurs. Thus, the calculated tunneling currents in CTS point to the importance of augmented carbon−sulfur conjugation (Table 3) in the enhancement of molecule−electrode coupling compared to the dithiol OPE benchmarks.

2.2. Resonant Currents. In the resonant regime, the electrode Fermi levels are resonant with molecular energies, and a ballistic

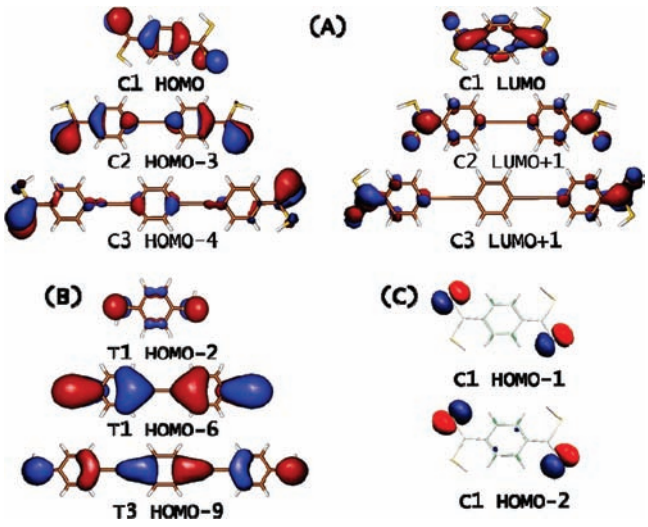

Figure 5. (A) Filled and empty MOs that show the strongest contributions (see Figure 4) to the current for CTS. (B) Filled MOs that show the strongest contributions (see Figure 4) to the current for DTS. Empty MOs give negligible contribution to the current for DTS and are not shown. (C) A pair of energetically close MOs with strong coupling to the electrode and with opposite phases whose contributions to the current destructively interfere.

Table 3. Resistance (in MΩ) for CT Systems with the Interaction of One of the Terminal Sulfurs with the Electrodes Turned off[a]

system	C1	C2	C3
LS1:RS1	2.4819×10^5	6.7417×10^6	1.2994×10^8
LS1:RS2	3.7492×10^4	5.4714×10^5	1.3455×10^7
LS2:RS1	3.7473×10^4	5.5459×10^5	1.3252×10^7
LS2:RS2	4.0122×10^3	4.4179×10^4	1.1703×10^6

[a] In these computations, the carbodithioate moiety was treated as a linker in which one sulfur features a single bond to the terminal carbon (S1) while the other features a full C−S double bond (S2). L and R represent right and left contacts to the electrodes. Thus LS1:RS2, for example, represents a system where only the single bonded sulfur is coupled to the left electrode and only the double bonded sulfur is coupled to the right electrode.

current flows through the molecule. Intuitively, this current should depend only on the contact resistance as defined by the coupling strength of each MO to the electrodes. We can define the resonant current through MO m using eq 5 and, in analogy with eq 8a, as:

$$I_m^{\mathrm{Res}} = \left(\frac{q}{h}\right)\int_{E_{Low}}^{E_{High}} \sum_n \times \frac{\Gamma_{mn}^L \Gamma_{nm}^R}{\left[E - E_m + \frac{i}{2}(\Gamma_{mm}^L + \Gamma_{mm}^R)\right]\left[E - E_n - \frac{i}{2}(\Gamma_{nn}^L + \Gamma_{nn}^R)\right]} \times [f_L(E) - f_R(E)]dE \quad (9)$$

The integration extends over the line width $\Gamma_{mm}^L + \Gamma_{mm}^R$ associated with molecular orbital m with energy E_m: $E_{Low} = E_m - 0.5(\Gamma_{mm}^L + \Gamma_{mm}^R)$;$E_{High} = E_m + 0.5(\Gamma_{mm}^L + \Gamma_{mm}^R)$ and the Fermi level is assumed to be resonant with the energy of the orbital ($E_F = E_m$). In this orbital approximation, virtual oxidized or reduced states of the bridge are treated in an orbital approximation, so virtual state lifetimes appear as orbital energy linewidths. The sulfur−gold coupling parameter is $\gamma = 0.1$ eV. In the tunneling regime, the conductance mediated by an MO depends on both the energy separation between the MO and the Fermi level and the strength of the coupling between the MO and the electrodes. However, in the resonant regime, the conductance depends only on the strength of the broadening matrix elements (the energy line width over which the current is integrated in eq 9). In our calculations, we find that contributions from off resonant cross terms ($n \neq m$) are negligible in the summation of the integrand in eq 9, and the summation is always positive. This further simplifies the picture, as the currents in eq 9 are the intrinsic contributions of orbital m, free of any interference from other MOs. As the Fermi level approaches resonance with the HOMO or LUMO, the orbital nearest E_F, will dominate ballistic transport ($I^{\mathrm{Res}} = I_m^{\mathrm{Res}} m =$ HOMO/LUMO). Table 4 shows the resonant current ($I^{\mathrm{Res}} = I_m^{\mathrm{Res}}$ for $V = 100$ mV) for CTS and DTS. The data in Table 4 clearly indicate that the HOMO for CTS is more strongly coupled to the electrodes than that for the corresponding DTS, producing higher ballistic currents in the resonant regime.

Table 4. Resonant current ($I_m^{\mathrm{Res}}(m =$ HOMO/LUMO) for $V = 100$ mV) for CTS and DTS

system	$I_{m=\mathrm{HOMO}}^{\mathrm{Res}}$ (μA)	system	$I_{m=\mathrm{HOMO}}^{\mathrm{Res}}$ (μA)
C1	74	**T1**	37
C2	26	**T2**	4.1
C3	24	**T3**	0.7

system	$I_{m=\mathrm{LUMO}}^{\mathrm{Res}}$ (μA)	system	$I_{m=\mathrm{LUMO}}^{\mathrm{Res}}$ (μA)
C1	42	**T1**	2.4
C2	35	**T2**	0.1
C3	25	**T3**	23

2.3. Mixed Mechanisms: Combinations of Tunneling and Resonant Currents. The measured β value of 0.05 Å^{-1} suggests an effective charge injection barrier height $< k_B T$ (k_B is Boltzmann's constant and T the temperature, 300 K) for the carbodithioate-terminated OPEs, indicating that tunneling transport likely competes with thermally activated carrier injection.[37,41,97] Recent studies indicate that conformational fluctuations can bias individual members of an ensemble toward one mechanism or another.[98,99] We show in this section that indeed such a competition between transport mechanisms is at play in our experiments. However, our analysis shows that very small charge injection barriers $< k_B T$ are not a prerequisite to produce the low β values seen in our experiments. Such small barriers require small β values only in the limit where broadening of the MO energies due to coupling to the electrodes is negligible. For negligible broadening, the transmission function $T(E)$ in eq 5 would be sharply peaked at the MO energies. Resonant contributions to the current from an MO are thus significant only when the separation between the Fermi level and the MO energies is within the line width ($\sim k_B T$) of the function $f_L(E) - f_R(E)$ in eq 5. On the other hand, when broadening of the MO energies due to coupling with the electrodes is non-negligible, the finite linewidths of the peaks in $T(E)$ and the thermal width of the difference function $f_L(E) - f_R(E)$ in eq 5 tend to increase the range of separations between the Fermi level and MO energies at which resonant transport become significant. By calculating the combined tunneling plus ballistic transmission using eqs 4 and 5, we show that the small β values observed

(97) Bixon, M.; Jortner, J. *J. Chem. Phys.* **1997**, *107*, 5154–5170.
(98) Berlin, Y. A.; Kurnikov, I. V.; Beratan, D.; Ratner, M. A.; Burin, A. L. In *Long-Range Charge Transfer in DNA II*; Springer-Verlag Berlin: Berlin, 2004; Vol. 237, pp 1−36.
(99) Hatcher, E.; Balaeff, A.; Keinan, S.; Venkatramani, R.; Beratan, D. N. *J. Am. Chem. Soc.* **2008**, *130*, 11752–11761.

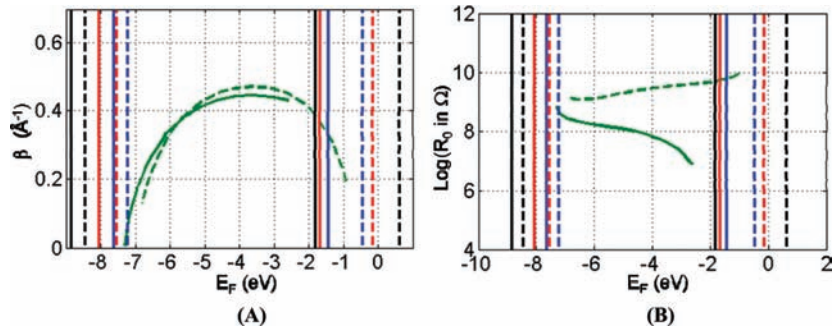

Figure 6. Change in (A) the decay constant β and (B) contact resistance R_0 as a function of Fermi energy E_F of the electrodes. The scans shown are for $\gamma = 0.1$ eV. Solid (dashed) green lines represent data for CTS (DTS). The vertical lines represent HOMO/LUMO energies for **C1/T1** (black), **C2/T2** (red), and **C3/T3** (blue) systems.

experimentally can result from barriers $\gg k_BT$ as a result of the competition between tunneling and resonant processes. Since neither the Fermi energy location relative to the molecular eigenstate energies, nor the details of the linker interactions with gold are known precisely, we treat E_F and γ as parameters and study the dependence of β and R_0 on these parameters. E_F is restricted to energies in the HOMO−LUMO gap, for cases where the Fermi energy lies 0.4−0.6 eV away from these orbitals; these boundaries on the E_F energy level ensure that the current/voltage dependence in the applied bias range of 100 mV is linear and that the conductance can be calculated directly from the slope of the $I-V$ plots. The sulfur−gold coupling parameter γ is varied over several orders of magnitude (Figure S2, SI), while maintaining the weak coupling limit.

Figure 6 shows the dependence of the effective contact resistance R_0 and the electronic coupling constant β on E_F in the HOMO/LUMO gap. The dependence of β on E_F in the HOMO/LUMO gap is theoretically well-known from extensive studies on hydrocarbon bridges.[100,101] β is expected to become larger as the E_F energy level becomes further removed from the frontier orbital energies. Asymmetries in the decay can be introduced due to the interfering contributions of many filled and/or empty MOs. This is precisely the case for CTS and DTS where the frontier orbitals (shown by dashed and solid vertical lines in Figure 6) do not even give the strongest contributions in the tunneling limit (Figure 4). The situation is more complicated for CTS, as the LUMO shifts to higher energies (Figure 6) with augmented OPE conjugation length; note that this behavior contrasts that of the CTS HOMO, and the observed HOMO and LUMO shifts for DTS, which shift to more favorable energies (CTS and DTS HOMOs shift to higher energies and DTS LUMO shifts to lower energies) with increasing conjugation. This effect results in an increase in β for CTS as E_F comes within ~0.6 eV of the LUMO energy (data not shown). Similarly, the dependence of the contact resistance on E_F for both systems is complex, because of the contributions from many different MOs. While the β values for the two linker systems remain close within the HOMO−LUMO midgap region (varying from 0.45 to 0.15 Å^{-1} at E_F values of -6.5 eV $< E_F < -2.5$ eV; Figure 6A), the CTS system is theoretically capable of achieving very low β values (<0.1 Å^{-1}) even in the weak sulfur−gold coupling limit ($\gamma = 0.1$ eV) as E_F approaches the HOMO. Moreover, the relative contact resistance value (R_0) of CTS is always lower (ranging from 5−180 times) than that of DTS for all values of E_F considered in Figure 6; note that R_0 varies by 2 orders of magnitude for CTS, and approximately an order of magnitude for DTS as the Fermi energy is varied within the HOMO−LUMO gap. These observations are consistent with the order of magnitude increase in resistance of DTS relative to CTS highlighted in the experimental data. The computations suggest that, in the weak coupling limit, the differences in resistance values between CTS and DTS could be increased (decreased) by shifting the Fermi level toward the LUMO (HOMO).

A similar analysis was performed for the dependence of R_0 and β on the sulfur−gold coupling parameter γ, at fixed values of the Fermi energy E_F. The results (Figure S2, SI) show that β is insensitive to changes in γ over several orders of magnitude. Also, the R_0 difference between CTS and DTS is independent of γ over several orders of magnitude, while R_0 decreases quadratically with increases in γ. However, the dependence of R_0 and β on the Fermi energies in the HOMO−LUMO gap are more complicated (β is sensitive to γ; change in R_0 with γ is not quadratic), especially for Fermi energies for with $E_F - E_m \approx \gamma$. A more detailed discussion is presented in section 2.2 of the SI.

Having explored the dependence of the conductance, contact resistance, and decay constant on our modeling parameters, we now address the question of whether our theoretical approach in the weak sulfur−electrode coupling regime explains our experimental data. The experiments show low β values (~0.11 Å^{-1} for DTS and ~0.05 Å^{-1} for CTS), which is plausible when the Fermi energy is close to a frontier orbital, and both tunneling and resonant currents contribute. β values as low as ~0.05 Å^{-1} for the CTS can be realized from the plots of β vs E_F in Figure 6(A) only if the Fermi level lies close to the filled orbitals for the CTS. While the ordering of the LUMO energies for the CTS (C1 < C2 < C3) tends to make β large as E_F shifts toward the empty orbitals, the ordering of the HOMO energies for both CT and DT OPEs (C1 < C2 < C3 and T1 < T2 < T3) tends to reduce β as E_F shifts toward the filled orbitals. Since both linker systems couple to the electrodes through a sulfur−gold bond, we expect the Fermi levels for both systems to be close energetically. However, near the HOMO energy (Figure 6A), the CTS show a larger β value than the DTS at the same E_F, in contrast to the experimental values. These data suggest that the Fermi level might be pinned at different energies for CT and DT OPEs. The physical basis for this assumption arises from differences at the linker−electrode interface. The π-conjugated sulfur atoms of the carbodithioate group likely serve to modify the contact considerably with respect to the thiol function, altering the alignment between the Fermi level with the HOMO/

(100) Beratan, D. N.; Hopfield, J. J. *J. Am. Chem. Soc.* **1984**, *106*, 1584–1594.
(101) Onuchic, J. N.; Beratan, D. N. *J. Am. Chem. Soc.* **1987**, *109*, 6771–6778.

LUMO of the OPE molecules. Both the extent of delocalization and the number of terminal sulfurs connected to the conjugated molecular cores differ in DTS and CTS, leading to differences in the orbital symmetry and energy levels that mediate the coupling. Such an end group effect on the alignment of MOs with the Fermi level has been invoked previously to explain the different decay constants for the thiol and pyridine-terminated carotenoid molecular junctions.[43]

Our calculations show that a hole injection barrier (separation between the Fermi level and the filled MOs) of ~0.4 eV, is sufficient to produce the experimentally observed low β values. The value of ~0.4 eV is an upper limit for the barrier at which resonant transport processes start competing with tunneling transport, significantly lowering the β value. Note that this barrier value is an upper limit due to the assumption of coherent transport; incoherent transport resulting from the coupling of the charge to molecular and solvent vibrational degrees of freedom would lead to a smaller barrier.

Conclusion

We have probed single-molecule conductances in phenylene−ethynylene molecules terminated with thiol and carbodithioate linkers, using STM break-junctions and nonequilibrium Green's function analysis. Experimental data demonstrate that the carbodithioate linker not only augments electronic coupling relative to thiol, but reduces the effective barrier for charge transport, making possible mixed tunneling/hopping transport mechanisms, and underscoring that *phenylene−ethynylene-based molecular wires are more highly conductive than originally appreciated*. Theoretical analysis considered three regimes of charge transport: tunneling, the resonant conduction, and a mixed regime where both tunneling and resonant transport processes operate. Interestingly, for the tunneling regime, the frontier molecular orbitals are not the major tunneling current mediators. Independent of the mechanism of charge transport, the carbodithioate-terminated systems (CTS) show larger conductances than do the analogous thiol-terminated systems (DTS). We predict that this trend will be retained in general for other metal and semiconducting electrodes which couple weakly to conjugated organic molecules via a thiol linker: replacement of thiol with carbodithioate will augment electronic coupling and reduce the effective barrier for charge transport. Our calculations further suggest that the experimental data can be explained via a weak coupling limit analysis in which the Fermi energies lie close to those of the CTS/DTS filled orbitals, such that a mix of tunneling and resonant transport mechanisms operate. Our calculations suggest an upper limit of ~0.4 eV for the charge injection barrier, at which resonant transport processes become competitive with tunneling transport to produce the low values of β observed experimentally in our systems. Collectively, these experimental and theoretical data emphasize the promise for using carbodithioate-based linkers in molecular electronics applications.

Acknowledgment. We thank Dr. NongJian Tao and Dr. Yufan He for useful discussions. We thank Prof. Jeffery R. Reimers for providing the CNDO program. Financial support from the National Science Foundation (NSEC DMR04-25780, CHE-0628169, and CHE-0628218) is gratefully acknowledged. M.J.T. is grateful to the Francqui Foundation (Belgium), and VLAC (Vlaams Academisch Centrum), Centre for Advanced Studies of the Royal Flemish Academy of Belgium for Science and the Arts, for research fellowships.

Note Added after ASAP Publication. This article posted on April 30, 2010 with incomplete corrections. The corrected version published May 19, 2010.

Supporting Information Available: Synthetic procedures; characterization and spectroscopic data; theoretical and computational details; complete references 35 and 87. This material is available free of charge via the Internet at http://pubs.acs.org/.

JA909559M